Available online at www.sciencedirect.com
ScienceDirect
Geotextiles and Geomembranes 26 (2008) 317–334
Geotextiles and Geomembranes
www.elsevier.com/locate/geotexmem

Effects of viscous behavior of geosynthetic reinforcement and foundation soils on the performance of reinforced embankments ☆

Allen Lunzhu Li[a,b,*], R. Kerry Rowe[c,1]

[a]*Key Laboratory of Southwest Natural Resource Exploitation and Environmental Disaster Control Engineering, China Ministry of Education and Chongqing University, P.R. China*
[b]*Golder Associates Ltd., 2390 Argentia Road, Mississauga, Ontario, Canada L5N 5Z7*
[c]*Queen's University, Kingston, Ontario, Canada K7 K 3N6*

Received 27 August 2007; received in revised form 29 November 2007; accepted 6 December 2007
Available online 20 February 2008

Abstract

The combined effects of viscoelastic behavior of geosynthetic reinforcement and viscoplastic nature of rate-sensitive foundation soils on the performance of reinforced embankments are investigated. The variation of viscoelastic properties is examined using geosynthetic products that are made of polyester, polypropylene and polyethylene. The foundation soils consist of two soft clay deposits with different strain-rate sensitivities. Embankment construction is numerically simulated to identify the magnitude of creep deformation of the reinforcement and the foundation soil under both limit state and working stress conditions and the consequent effects on the stability of the embankment. It is shown that the creep of geosynthetic reinforcement and foundation soil can decrease the short-term stability of embankments and that the mobilized reinforcement stiffness and corresponding tensile force can be significantly lower than that measured from standard laboratory test. The isochronous stiffness can reasonably represent the mobilized reinforcement stiffness at the critical stage of the embankment. During post-construction periods, reinforcement strain can increase substantially and it has shown that the increase in reinforcement strain is largely due to the viscoplastic behavior of foundation soils. The mobilized reinforcement strain under working stress conditions with respect to reinforcement stiffness are also discussed.

Keywords: Reinforced embankment; Geosynthetic reinforcement; Creep; Viscoelasticity; Soft soil; Stability

1. Introduction

Geosynthetics reinforcement is often needed to allow construction of embankments on soft clayey foundations (e.g. Hinchberger and Rowe, 2003; Varuso et al., 2005; Sarsby, 2007; Bergado and Teerawattanasuk, 2008; Rowe and Taechakumthorn, 2008). This reinforcement is typically made from polyester (PET), polypropylene (PP) or polyethylene (PE) and all are susceptible to creep to some extent (e.g. McGown et al., 1982; Shrestha and Bell, 1982; Allen et al., 1982; Christopher et al., 1986; Greenwood and Myles, 1986; Jewell and Greenwood, 1988; Leshchinsky et al., 1997; Bueno et al., 2005). It is also well known that natural soft cohesive soil deposits exhibit significant time-dependent behavior and the undrained shear strength of natural soft clays is strain rate dependent (e.g. Casagrande and Wilson, 1951; Bjerrum, 1972; Graham et al., 1983; Leroueil and Marques, 1996; Sheahan et al., 1996).

The viscoelastic nature of geosynthetics can have a significant effect on the performance of reinforced soil embankments constructed on inviscous foundation soils (Li and Rowe, 2001). The mobilized reinforcement stiffness at the end of embankment construction can be significantly lower than the stiffness that is measured using standard wide-width tensile tests. Li and Rowe have shown that the isochronous stiffness of reinforcement can reasonably

☆Professor S.A. Tan served as Editor for the review of this paper.

*Corresponding author at: Key Laboratory of Southwest Natural Resource Exploitation and Environmental Disaster Control Engineering, China Ministry of Education and Chongqing University, P.R. China. Tel.: +1 905 567 4444.
E-mail addresses: ali@golder.com (A. Lunzhu Li), kerry@civil.queensu.ca (R. Kerry Rowe).
[1]Tel.: +1 613 533 6933; fax: +1 613 533 6934.

0266-1144/$ - see front matter © 2007 Elsevier Ltd. All rights reserved.
doi:10.1016/j.geotexmem.2007.12.002

represent the end of construction stiffness if the foundation soils are inviscous (i.e. rate-insensitive). Given issues such as creep deformations and creep rupture of geosynthetic reinforcement, a number of investigators (e.g. Bonaparte and Berg, 1987; Jewell and Greenwood, 1988; Allen, 1991) have recommended designing based on the long-term allowable strength of the reinforcement.

The viscoplastic behavior of rate-sensitive foundation soils can also have a significant effect on the performance of reinforced embankments (Rowe and Li, 2002). Since the strain mobilized in reinforcement increases with time due to creep of a rate-sensitive foundation soil, the allowable embankment height should be based on a mobilized undrained shear strength that reflects typical strain rates mobilized in the field during construction rather than the strain rate in traditional tests used to establish the "measured" undrained shear strength (Li and Rowe, 2002).

Although the effects of rate-sensitivity and creep have been examined separately for reinforcement and foundation soil, there is paucity of literature dealing with the combined effects of creep of the geosynthetic reinforcement and foundation soil on reinforced embankment behavior. Thus, the objective of this paper is to explore the potential combined effect of the viscoelastic properties of geosynthetic reinforcement and viscoplastic properties of the foundation soils under both short- and long-term conditions.

2. Finite element modeling and constitutive model parameters

A typical four-lane highway embankment with 2h:1v side slopes was considered. The embankment overlies a 15-m soft cohesive deposit underlain by a relatively permeable layer. The finite element mesh is shown in Fig. 1. The centerline of the embankment and the far field lateral boundary (located 100 m from the centerline) were taken to be smooth and rigid. The bottom of the finite element mesh was assumed to be rough and rigid and zero excess pore pressures were assigned to the nodes along the bottom boundary line.

The geosynthetic reinforcement was modeled using two-noded bar elements and a one-dimensional viscoelastic constitutive model as described in Section 2.1. Two-noded joint elements governed by a Mohr–Coulomb failure criterion (Rowe and Soderman, 1987) with a friction angle $\phi' = 37^\circ$ and zero cohesion were used for the embankment fill/reinforcement interface.

A total of 1594 linear strain triangular elements (3516 nodes) were used to discretize the embankment and foundation soils. A non-linear elastic, perfectly plastic, model with a Mohr–Coulomb failure surface and a non-associated flow rule (Davis, 1968) was adopted for the granular embankment fill (Section 2.2). An elasto-viscoplastic cap soil model (Chen and Mizuno, 1990; Rowe and Hinchberger, 1998), as described in Section 2.3, was adopted for the foundation soil.

The constitutive models outlined above were implemented in a modified version of finite element program AFENA (Carter and Balaam, 1990). Embankment construction was simulated by turning on the gravity of the fill in 0.75-m thick lifts at a rate corresponding to the embankment construction rate (CR).

2.1. Constitutive model for geosynthetic reinforcement

The model adopted in this paper is based on the non-linear viscoelastic multi-Kelvin model proposed by Zhang and Moore (1997). The advantage of their multi-Kelvin model is that only a few material constants are needed and the number of Kelvin elements can be modified as necessary to model creep over different time periods. Each Kelvin element in the model is comprised of a spring and dash pot and these elements can be assembled in series (Fig. 2) with each element having a different spring stiffness and dashpot viscosity.

When the reinforcing element is subject to an increment in stress, $\dot{\sigma}$, which brings the total tensile stress to σ, the increment in strain in the reinforcement, $\dot{\varepsilon}$, is the sum of instantaneous elastic strain increment, $\dot{\varepsilon}^{e}$, and time-delayed viscoelastic strain, $\dot{\varepsilon}^{v}$, i.e.

$$\dot{\varepsilon} = \dot{\varepsilon}^{e} + \dot{\varepsilon}^{v}, \tag{1}$$

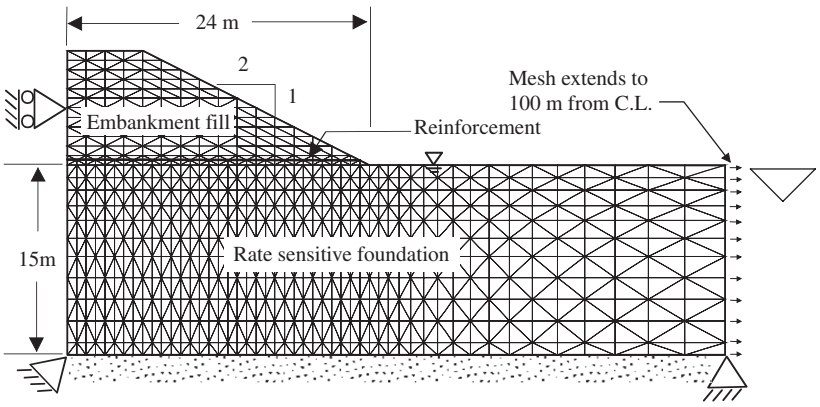

Fig. 1. The finite element mesh and geometry of the system.

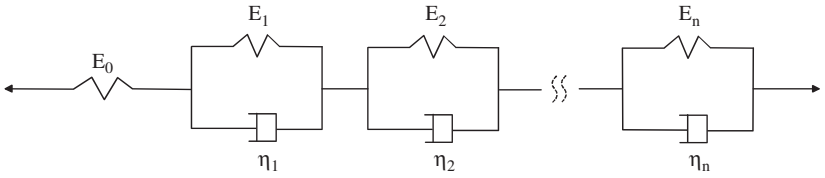

Fig. 2. Viscoelastic model with multi-Kelvin elements.

Table 1
Four types of geosynthetic reinforcement examined and their ultimate strength and stiffness

Designated symbol	Geosynthetic materials				
	Reinforcement type	Polymer type	Manufacturing process	Ultimate strength (kN/m)	Stiffness $J_{5\%}$ (kN/m)
G1	Geogrid	HDPE	PSD[a]	72	850
G2	Geogrid	HDPE	PSD	166	1940
G3	Geotextile	PP	Woven	186	1578
G4	Geotextile	PET	Woven	200	1736

$J_{5\%}$, reinforcement stiffness at 5% strain determined from a standard wide-width tensile test at a strain rate of 10% min^{-1}.
[a]PSD, punched sheet drawn.

where $\dot{\varepsilon}^{e} = \dot{\sigma}/E_0$; and E_0 is the stiffness of the independent spring, which is the function of the tensile stress as follows:

$$E_0 = a_0 \exp(-a_1\sigma^3), \tag{2}$$

where a_0 and a_1 are material constants.

The viscous strain rate, $\dot{\varepsilon}^{v}$, is represented by

$$\dot{\varepsilon}^{v} = \sum_{i}^{n}\left\{\frac{\sigma}{(E_i\tau_i)} - \frac{\varepsilon_i^{v}}{\tau_i}\right\}, \tag{3}$$

where n is the number of Kelvin elements, $\tau_i = \eta_i/E_i$ denoted as the retardation time; E_i and η_i are the spring stiffness and the dashpot viscosity of the ith Kelvin element, respectively. The following equations are used to deduce the material constants E_i and τ_i:

$$E_i = (\alpha)^{i-1}E_1, \tag{4}$$

$$\tau_i = (\beta)^{i-1}\tau_1. \tag{5}$$

Thus, seven independent material constants, a_0, a_1, α, β, E_1, τ_1 and n are needed to define the viscoelastic reinforcement. The finite element formulation of the viscoelastic problem was derived based on the method proposed by Zienkiewicz (1977), which is similar to that for the incremental plasticity theory.

An uniaxial formulation of the proposed constitutive model for the reinforcement was implemented into AFENA (Li and Rowe, 2001). Finite element creep simulations were conducted to calibrate the viscoelastic model using laboratory creep test data of four typical geosynthetic reinforcement products, namely, a high density polyethylene (HDPE) geogrid G1 (Leshchinsky et al., 1997), a stronger HDPE geogrid G2 (data courtesy of Tensar Earth Technologies Inc.), a woven PP geotextile G3 (Greenwood, 1990) and a woven PET geotextile G4 (Greenwood, 1990). The mechanical properties are given in Table 1 and the viscoelastic parameters are given in Table 2. Fig. 3 shows that the predicted reinforcement creep strains using the Zhang and Moore model agree very well with the measured creep strain for all four geosynthetics.

Table 2
The viscoelastic model parameters

Designated symbol	Material constant						
	a_0 (kN/m)	a_1 (m/kN)	α	β	E_1 (kN/m)	τ_1 (h)	n
G1	1050	7.0×10^{-6}	1	10	3000	0.02	9
G2	2200	4.0×10^{-7}	1.1	10	6300	0.05	9
G3	1700	4.0×10^{-7}	0.99	10	9800	0.03	9
G4	1800	2.0×10^{-7}	1.2	10	60,000	0.05	7

2.2. Embankment fill parameters

The embankment fill was assumed to be a purely frictional granular soil with a friction angle $\phi' = 37^{\circ}$, dilatancy angle $\psi = 6^{\circ}$ and a unit weight $\gamma = 20\,kN/m^3$. The friction angle of the fill material has some effect on the ultimate height of the embankment but a lower friction angle (e.g. 32°) would have very little effect on the time-dependent deformation of the embankment and reinforcement since the creep deformations are governed by the viscoelastic properties of the geosynthetics and viscoplastic properties of the foundation soils.

The non-linear elastic behavior of the fill was modeled using Janbu's (1963) equation

$$\left(\frac{E}{P_a}\right) = K\left(\frac{\sigma_3}{P_a}\right)^{m}, \tag{6}$$

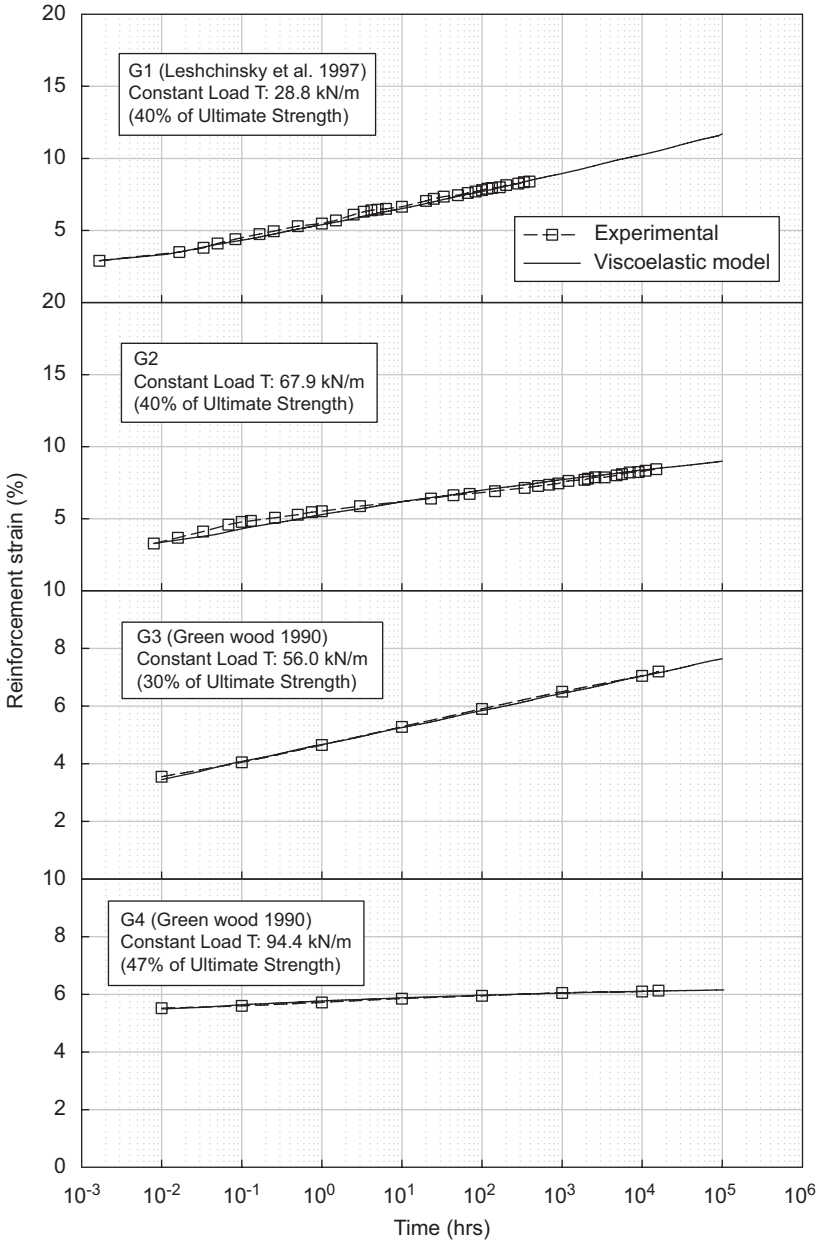

Fig. 3. Comparison of the calibrated and predicated creep strains with the measured creep strain for the four geosynthetic reinforcement products examined.

where E is the Young's modulus of the soil, P_a the atmospheric pressure, σ_3 the minor principal stress, and K and m are material constants selected to be 300 and 0.5, respectively. A higher modulus of the embankment fill material would have insignificant effect on the deformations of the embankment and reinforcement since the deformations of the embankment is largely due to the yielding of the foundation soil and creep of the both geosynthetic reinforcement and foundation soil.

2.3. Constitutive model for the foundation soils and soil properties examined

An elasto-viscoplastic cap soil model (Rowe and Hinchberger, 1998) with an elliptical yield cap (Chen and Mizuno, 1990) and Drucker–Prager failure criterion were adopted in conjunction with fully coupled Biot consolidation theory (Biot, 1941) for the foundation soil. The viscoplasticity was modeled based on Perzyna's (1963) theory. The model was calibrated and validated against both short- and long-term field behavior of a geotextile-reinforced embankment constructed over the rate-sensitive Sackville foundation soil (Rowe and Hinchberger, 1998) and the behavior of an unreinforced embankment constructed over the rate-sensitive Gloucester foundation soil (Hinchberger and Rowe, 1998). The main features of the model are summarized in the following text and Fig. 4. Additional details regarding the model are provided by Hinchberger (1996) and Rowe and Hinchberger (1998).

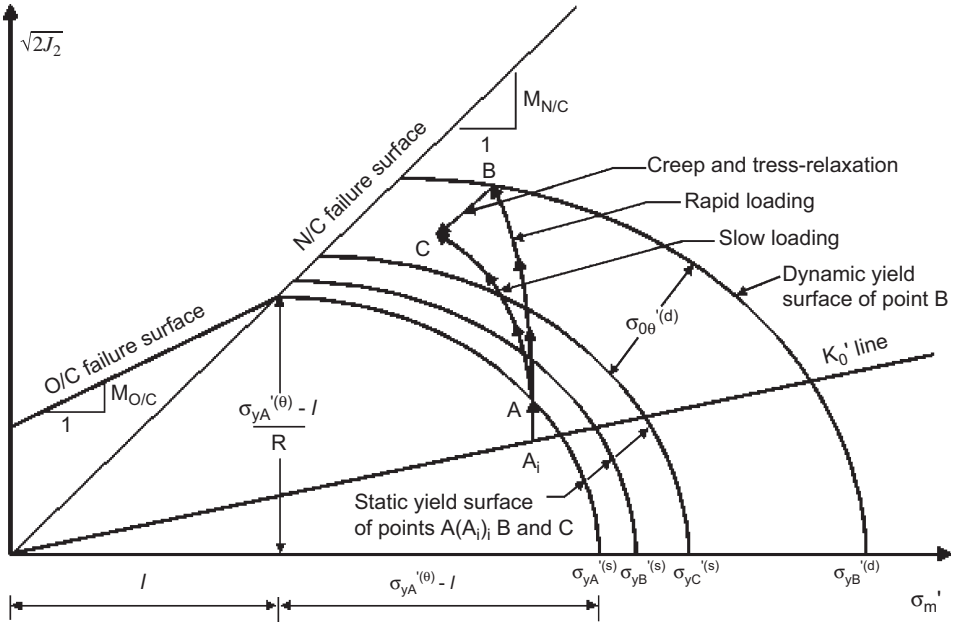

Fig. 4. Elasto-viscoplastic elliptical cap soil model (modified from Rowe and Hinchberger (1998)).

The yield surface of the elliptical cap model shown in Fig. 4 in $\sigma'_m - \sqrt{2J_2}$ stress space (where σ'_m is the mean effective stress, J_2 is the second invariant of the deviatoric stress tensor) can be characterized by the yield surface aspect ratio R, the center of the cap l, and the size of the static and dynamic yield envelope $\sigma'^{(s)}_y$ and $\sigma'^{(d)}_y$ (the intercept with the σ'_m axis). The failure is governed by the Drucker–Prager failure criterion having a slope $M_{N/C}$ and $M_{O/C}$ for the normally and overconsolidated failure envelope, respectively.

Since the deposition of the foundation soil, it has experienced "ageing" due to the secondary compression which has resulted in a higher preconsolidation pressure than the initial vertical effective stress (Bjerrum, 1972). This preconsolidation pressure is considered as the static preconsolidation pressure in terms of effective mean stress $\sigma'^{(s)}_y$ in the viscoplastic model. The stress state point, A_i shown in Fig. 4, represents an initially slightly over-consolidated point within a clayey foundation having a mean static preconsolidation pressure $\sigma'^{(s)}_{yA}$ and an earth pressure coefficient at rest K'_0. With rapid embankment loading under undrained conditions, the stress path moves up vertically with constant effective mean stress due to the undrained conditions until it reaches point A on the static yield surface, where the soil starts to yield. After the soil yields, it moves towards the failure envelope along a curved path to point B at the end of construction, where the soil is overstressed by an amount, $\sigma'^{(d)}_{os}$, and the positive viscoplastic volumetric strains expand the static yield envelope from $\sigma'^{(s)}_{yA}$ to $\sigma'^{(s)}_{yB}$. After the end of construction and before significant consolidation, creep and stress-relaxation of the soil skeleton cause the stress path to move from point B to C and the static yield envelope expands from $\sigma'^{(s)}_{yB}$ to $\sigma'^{(s)}_{yC}$ due to the positive viscoplastic volumetric strains. The consequent plastic deformation and excess pore pressure are a function of the overstress and the location of the stress state point on the dynamic yield envelope. The stress path A–C represents the possible stress path when the soil is under a slow embankment loading.

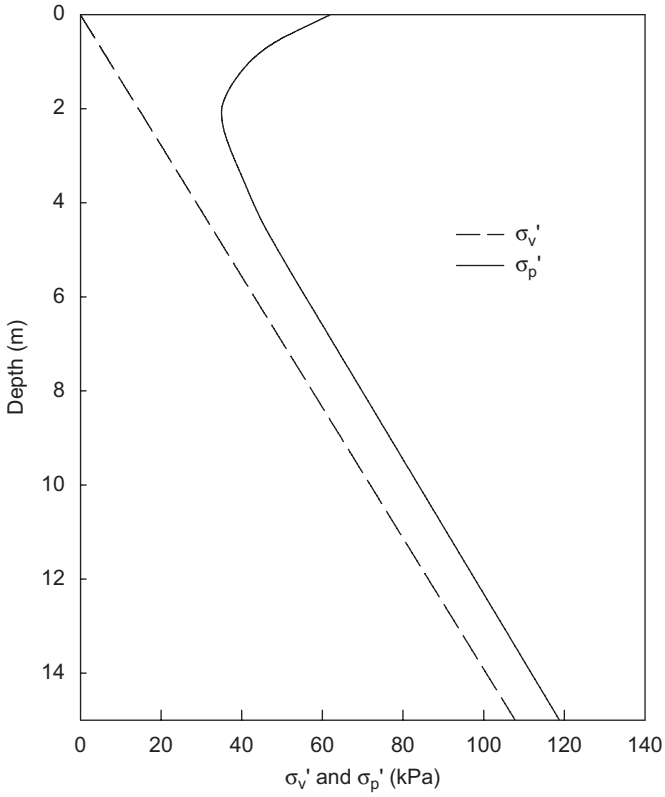

Fig. 5. Initial vertical effective stress and preconsolidation pressure profiles for both Soils R1 and R2.

The total strain rate tensor, $\dot{\varepsilon}_{ij}$, of the elasto-viscoplastic soil is expressed as

$$\dot{\varepsilon}_{ij} = \dot{\varepsilon}^{e}_{ij} + \dot{\varepsilon}^{vp}_{ij}, \tag{7}$$

where $\dot{\varepsilon}^{e}_{ij}$ is the elastic strain rate tensor and $\dot{\varepsilon}^{vp}_{ij}$ is the viscoplastic strain rate tensor.

The elastic strain tensor, $\dot{\varepsilon}^{e}_{ij}$, is governed by the elastic bulk modulus, K, and shear modulus, G, which are given by

$$K = \frac{1+e}{\kappa}\sigma'_{m}, \tag{8}$$

$$G = \frac{3(1-2v')K}{2(1+v')}, \tag{9}$$

where σ'_{m} is the mean effective stress, e the void ratio, κ the recompression index in the $e - \ln(\sigma'_{m})$ space and v' is the Poisson's ratio. The viscoplastic strain rate tensor, $\dot{\varepsilon}^{vp}_{ij}$, is given by

$$\dot{\varepsilon}^{vp}_{ij} = \gamma^{vp}\langle\Phi(F)\rangle\frac{\partial f}{\partial\sigma'_{ij}}, \tag{10}$$

Table 3
Elliptical cap soil model parameters

Soil parameter	Soil R1	Soil R2
Failure envelope, $M_{N/C}$ (ϕ')	0.96 (29°)	0.96 (29°)
Failure envelope, $M_{O/C}$	0.75	0.75
Aspect ratio, R	1.25	1.25
Compression index, λ	0.16	0.16
Recompression index, κ	0.034	0.034
Coefficient of earth pressure at rest, K'_0	0.75	0.75
Poisson's ratio, v'	0.3	0.3
Unit weight, γ (kN/m^3)	17.0	17.0
Initial void ratio, e_o	1.38–1.5	1.38–1.5
Viscoplastic fluidity, γ^{vp} (h^{-1})	2.0×10^{-5}	1.0×10^{-7}
Strain rate exponent, n	20	30

where γ^{vp} is the viscoplastic fluidity parameter with units of inverse time, f is the plastic potential function that equals the elliptical cap yield function or the Drucker–Prager failure function using an associated flow rule; $\Phi(F)$ is the flow function defined as follows:

$$\Phi(F) = \left(\frac{\sigma'^{(s)}_{y} + \sigma'^{(d)}_{os}}{\sigma'^{(s)}_{y}}\right)^{n}, \tag{11}$$

where n is the strain rate exponent.

Two viscous soft foundation soils, denoted as Soils R1 and R2 with the same static preconsolidation profile (profile R) but with different viscoplastic properties (R1 and R2) were examined in this paper. The static preconsolidation pressure,σ'_{p}, of Soils R1 and R2 is shown in Fig. 5. The elasto-viscoplastic model parameters are summarized in Table 3. Soil R1 has properties similar to the Sackville soil described by Rowe and Hinchberger (1998) with a liquid limit of 50%, plasticity index of 18% and natural water content of 53%, respectively. As shown in Fig. 5, it was slightly overconsolidated with an initial void ratio of 1.3–1.5 and a unit weight of 17.0 kN/m^3. The effect of strain rate on the undrained shear strength is shown in Fig. 6. The increase in undrained shear strength was about 16% per logarithm cycle of strain rate for strain rates between 0.005 and 100%/h. This rate of change in undrained shear strength with strain rate was reported by Graham et al. (1983) and Soga and Mitchell (1996) for a number of rate-sensitive clays.

Kulhawy and Mayne (1990) compiled data obtained from 26 different overconsolidated and normally consolidated clays and found that an average increase in undrained shear strength typically equalled 10% per logarithm cycle of strain rate as shown in Fig. 6. Soil R2 had the same properties as Soil R1 except for the viscoplastic parameters, γ^{vp} and n. This implies that Soils

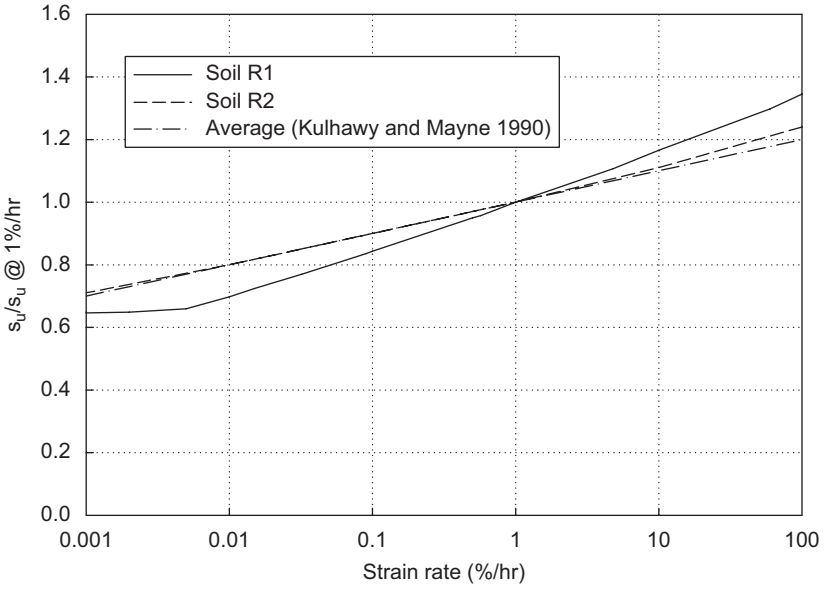

Fig. 6. Variation of the undrained shear of Soils R1 and R2 strength with strain rate.

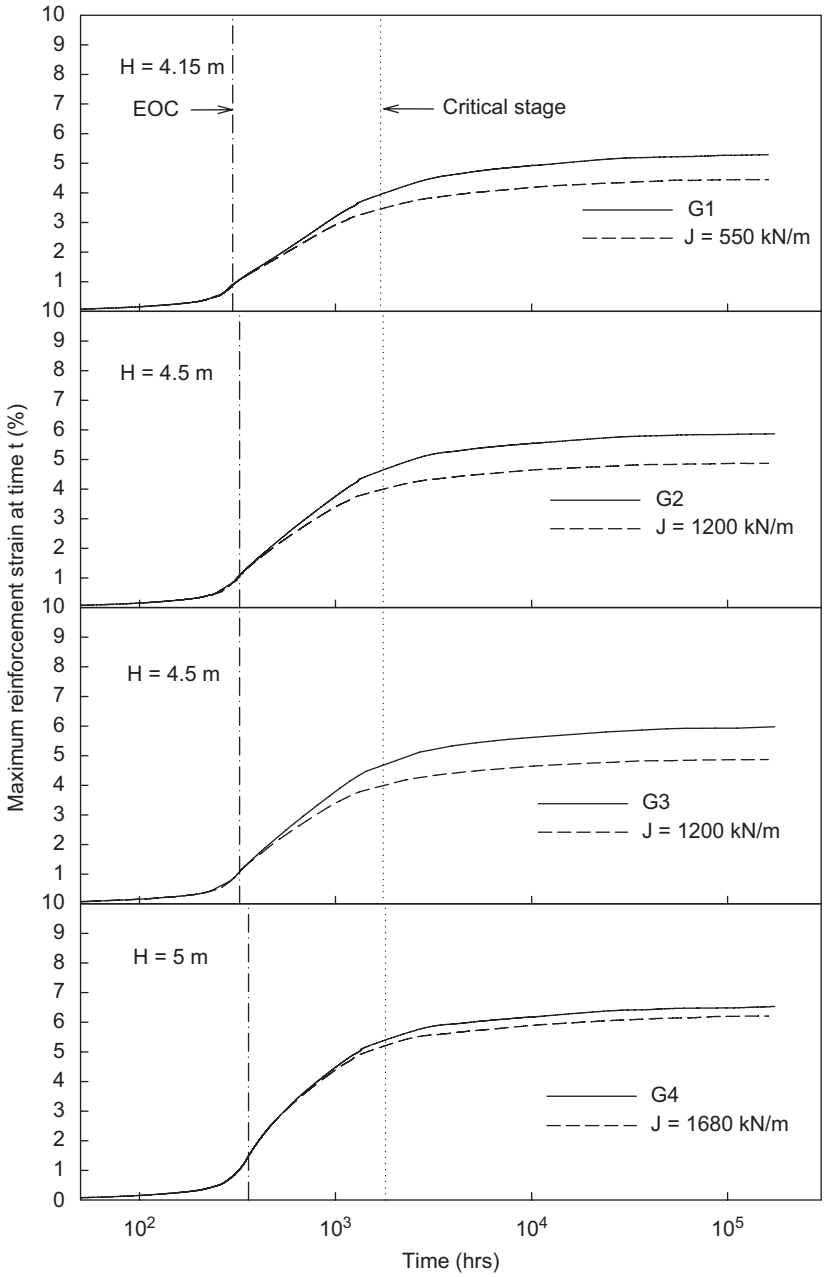

Fig. 7. The variation of reinforcement strain with time for embankments over Soil R1.

R1 and R2 have the same static undrained shear strength, which is the strength mobilized at an infinitesimal strain rate. The viscoplastic fluidity parameter, γ^{vp}, of Soil R2 was taken to be over two orders of magnitude lower than that of Soil R1. The viscoplastic constants of Soil R2 were selected to capture the average strain-rate sensitivity of typical soft clayey soils reported by Kulhawy and Mayne (1990) as shown in Fig. 6.

Groundwater table is assumed to be at the original ground surface. The hydraulic conductivity of soft clays was taken to be a function of void ratio,

$$k_v = k_{vo} \exp\left(\frac{e - e_o}{C_k}\right), \tag{12}$$

where k_{vo} is the reference hydraulic conductivity and is either 2×10^{-9} or 4×10^{-10} m/s, C_k is the hydraulic conductivity change index ($C_k = 0.75$) and e_o is the reference void ratio (taken to be 1.5). The hydraulic conductivity was considered to be anisotropic with $k_h/k_v = 4$.

3. Results and discussions

Numerical analyses were conducted to simulate construction of reinforced embankments on rate-sensitive foundation Soils R1 and R2. This paper reports the results from analyses for the embankments reinforced using the four geosynthetic products listed in Table 1. Typical

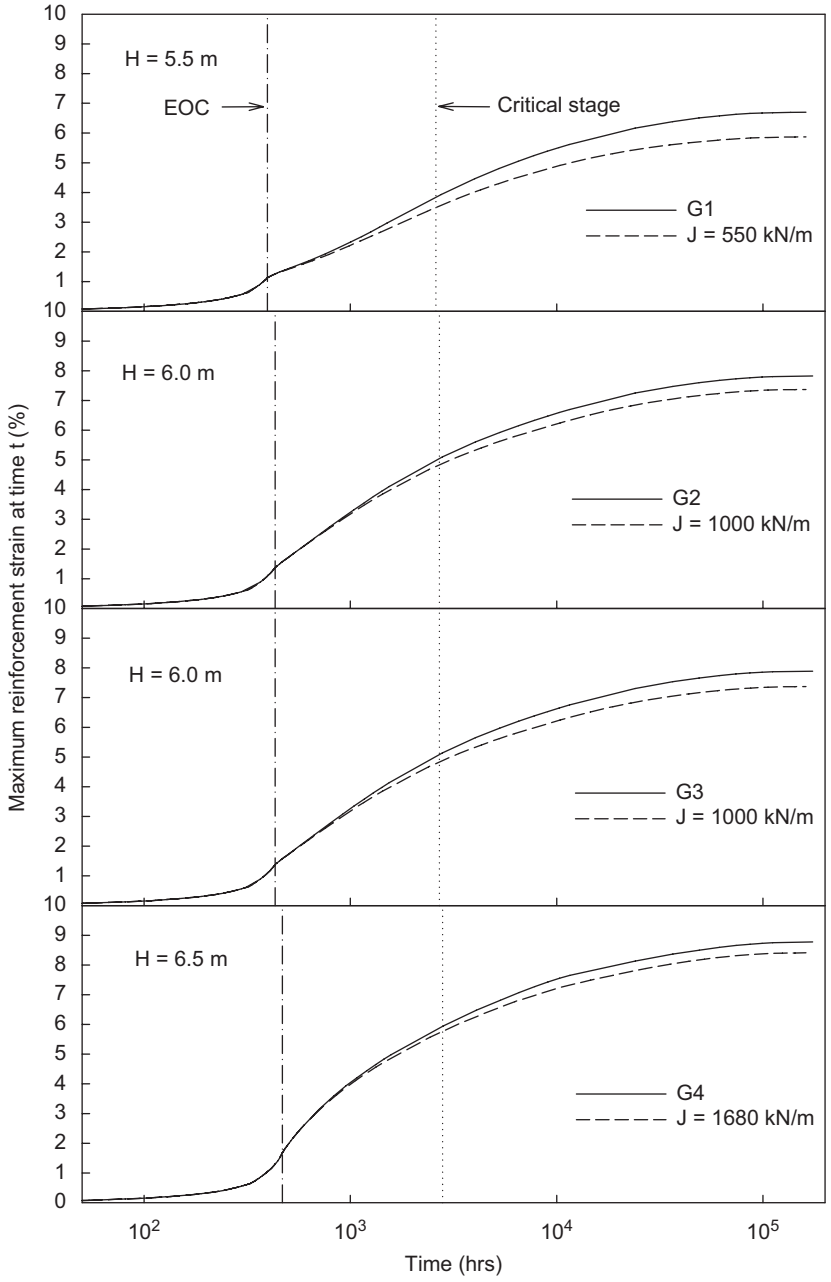

Fig. 8. The variation of reinforcement strain with time for embankments over Soil R2.

geosynthetic reinforcement has an allowable strain ranging between 4% and 7% (deduced using allowable strength and short-term stiffness from the GFR Specifier's Guide (2006) (Industrial Fabrics Association International 2006). For the embankments examined in this paper, an allowable reinforcement strain of 5% was adopted in the design.

3.1. Embankment heights based on mobilizing the full shear strength of the foundation soil

For embankments constructed over rate-sensitive soils, the critical stage in terms of stability is the time at which the excess pore pressure reaches maximum due to creep of the soil under a constant embankment load (Li and Rowe, 2002). This has been called the "critical stage" (Li and Rowe, 2002) and the critical strain rate (i.e. the strain rate corresponding to this "critical stage") controls the operational strength of foundation soils. The critical strain rates were calculated using numerical simulations of 5×10^{-5} and $1 \times 10^{-5}\,h^{-1}$ for embankments constructed over Soils R1 and R2, respectively. In addition to the undrained shear strength of the foundation soil, the embankment heights are also limited by the reinforcement force that corresponds to an allowable reinforcement

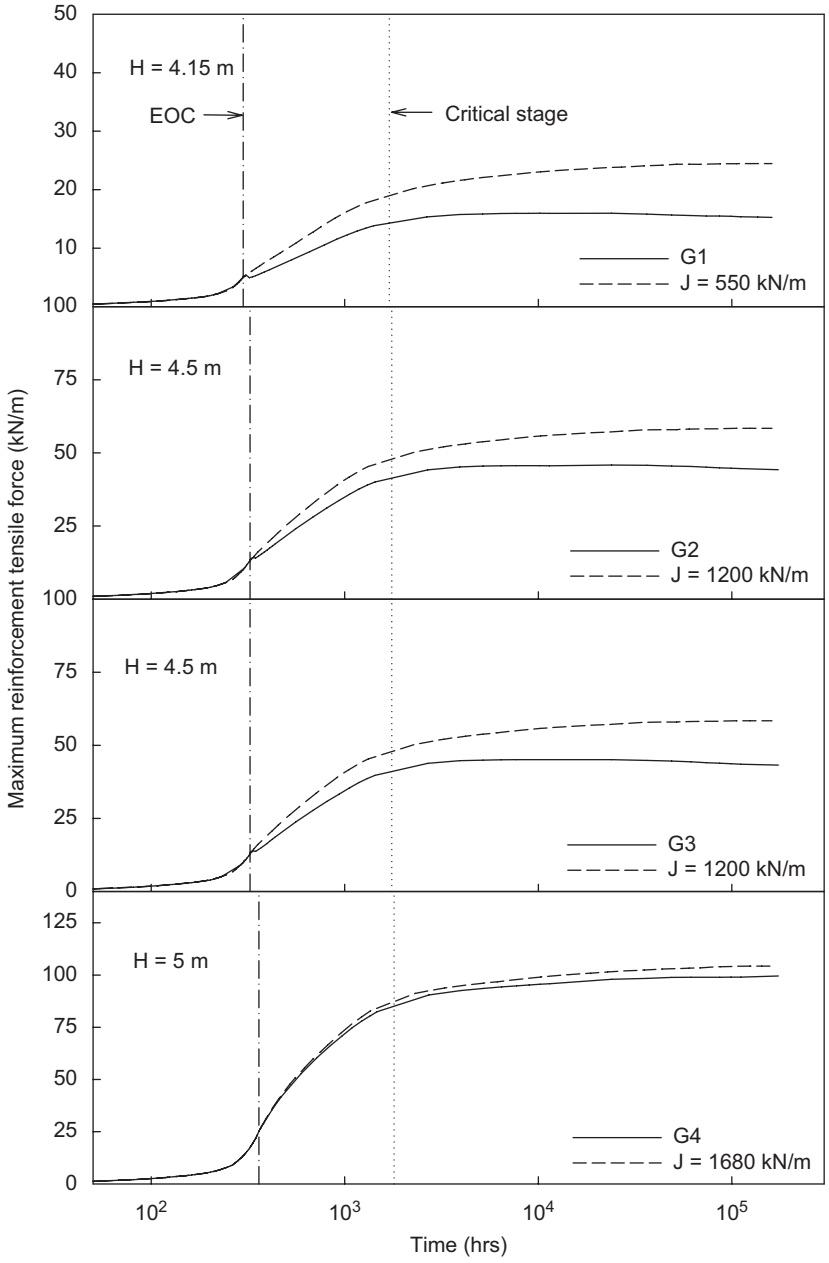

Fig. 9. The variation of reinforcement force with time for embankments over Soil R1.

strain. The embankments examined in this section were constructed to heights based on an allowable reinforcement strain of 5% at the critical stage. Since the reinforcement strain increases with time due to creep of the foundation soil (Rowe and Li, 2002), the embankments had to be constructed to heights at which the mobilized reinforcement strains are less than the allowable 5% at the end of construction. The height corresponding to 5% strain at the critical stage for different geosynthetic reinforcements were obtained from numerical simulations using an iterative procedure. The calculated embankment heights for the four types of reinforcement (G1, G2, G3 and G4) were 4.15 m for the lower strength geogrid (G1), 4.5 m for the higher strength geogrid (G2), 4.5 m for the woven PP (G3) and 5 m for the woven PET (G4) over Soil R1, and 5.5 m for the lower strength geogrid (G1), 6 m for the higher strength geogrid (G2), 6 m for the woven PP (G3) and 6.5 m for the woven PET (G4) over Soil R2.

3.1.1. Time-dependent behavior of reinforcement

The critical stage shown in Figs. 7–10 is slightly different for each case, however, the difference is barely visible. The case with viscoelastic reinforcement represented by the solid curve for each plot was used to define the critical stage.

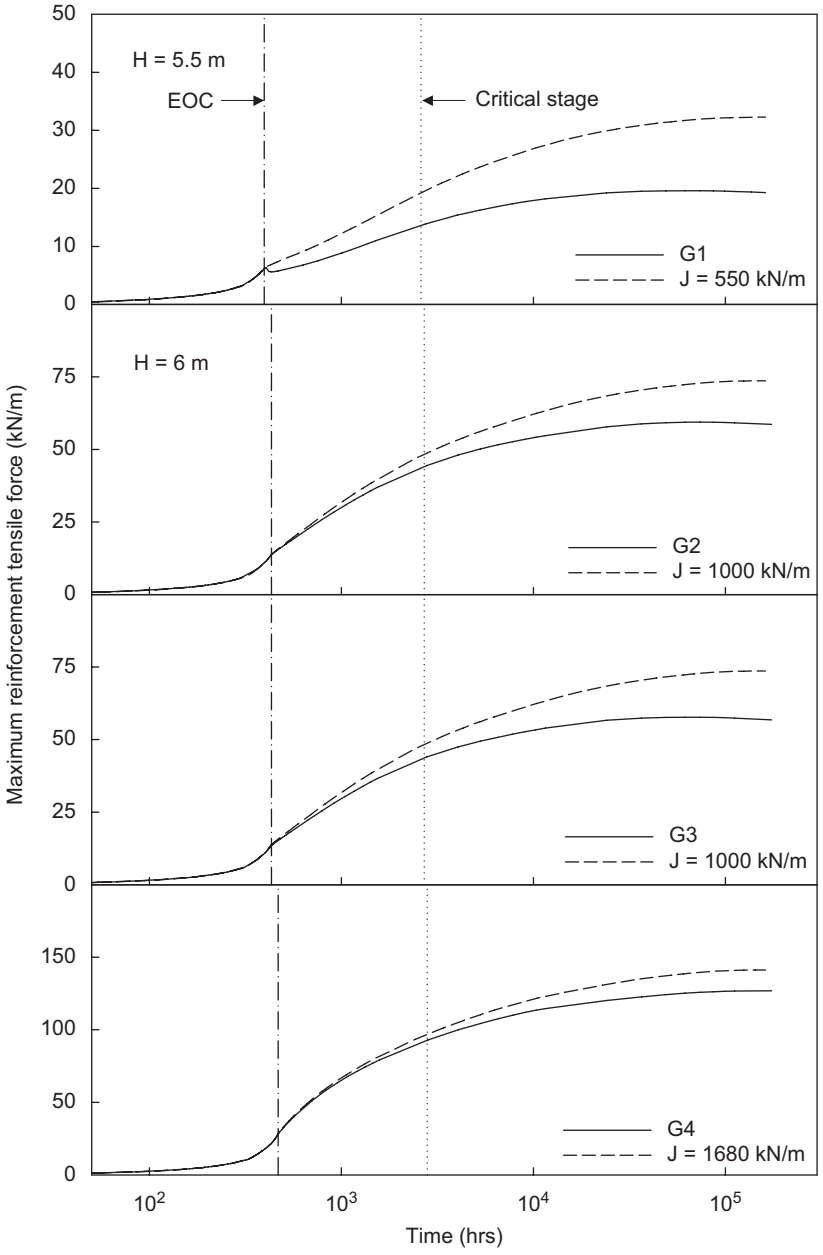

Fig. 10. The variation of reinforcement force with time for embankments over Soil R2.

Figs. 7 and 8 show the variation of the maximum reinforcement strain with time up to 98% consolation for embankments constructed over Soils R1 and R2, respectively. It can be observed that the maximum reinforcement strain was 1–2% at the end of construction, which was relatively low as a result of relatively high undrained shear strength of these rate-sensitive foundation soils mobilized due to rate effects. After construction, due to the creep of both foundation soils and reinforcement, the reinforcement strain increased to about 5% at the critical stage. After the critical stage, the reinforcement strain for embankments over Soil R1 increased moderately during consolidation of the foundation soil but was well below the limit strain for the reinforcement. In contrast, the reinforcement strain for embankments over Soil R2 increased significantly (approaching 9% in one case) over a relative long period of time during consolidation. The difference in response arises from the fact that Soil R2 was more viscous than Soil R1, consequently, Soil R2 experienced significant creep deformations during subsequent consolidation.

To differentiate the effects of creep of the reinforcement from that of the foundation soil, two additional series of analyses were conducted using inviscous reinforcement with stiffness the same as the mobilized stiffness of viscous reinforcement at the end of construction. Figs. 7 and 8 compare the time-dependent strain of the inviscous

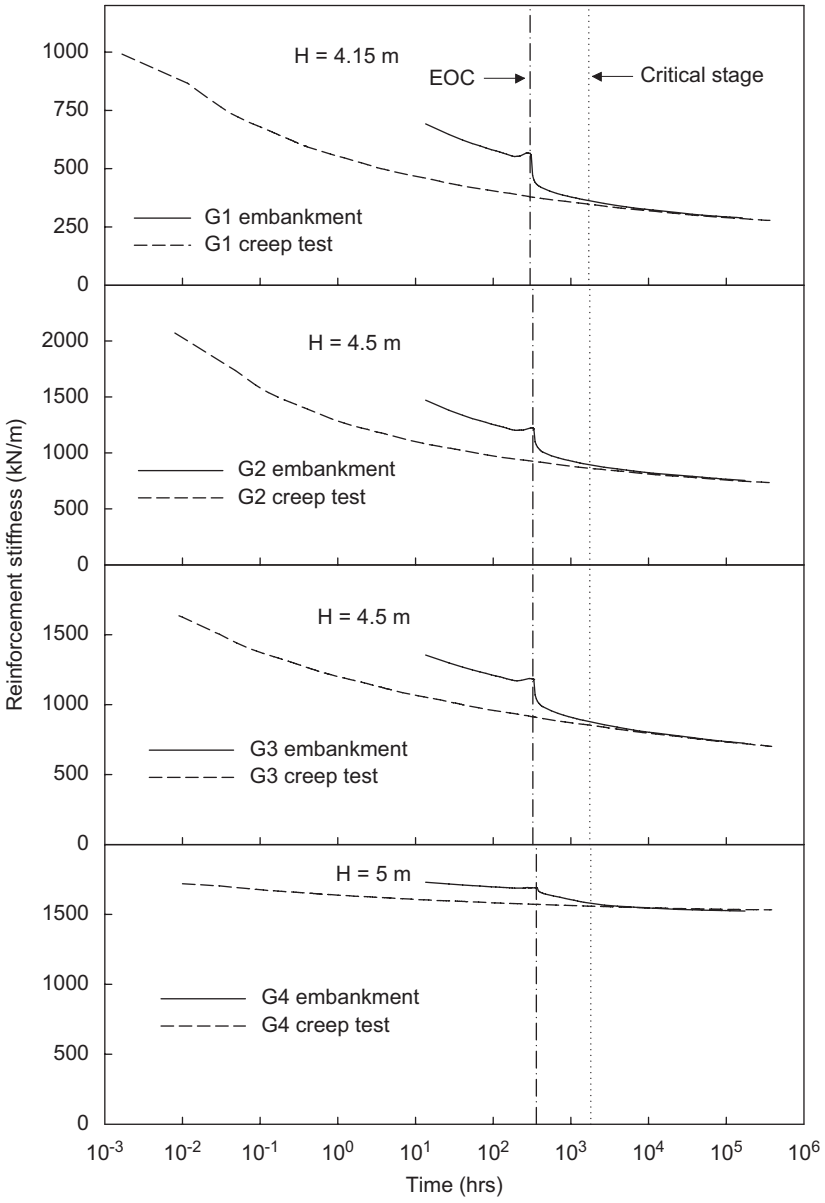

Fig. 11. The variation of reinforcement stiffness with time for embankments over Soil R1.

reinforcement to the strain of the viscous reinforcement. The difference in strain at 98% degree of consolidation for the viscous and inviscous reinforcement was about 0.5–1% for the embankments reinforced with the geogrids or the woven PP geotextile (G1, G2 and G3) for the two rate-sensitive foundation soils. For the woven PET reinforcement (G4), the effect of creep in reinforcement was insignificant. Thus, the creep of the foundation soils after the end of construction dominated the time-dependent reinforcement strain. In addition, the horizontal deformations of the foundation soil due to stress redistribution during consolidation also partially attributed to the post-construction reinforcement strain (Li and Rowe, 2001).

Figs. 9 and 10 show the variation of reinforcement force with time for embankments over Soils R1 and R2, respectively. Comparing the force mobilized in the viscous reinforcement to that in inviscous reinforcement, it can be seen that the stress relaxation was most significant for the lower strength geogrid reinforcement (G1). Stress relaxation of the higher strength geogrid and woven PP geotextile (G2 and G3) were moderate and the stress relaxation was insignificant for the woven PET geotextile (G4). Nevertheless, after the critical stage, the total force mobilized in the geogrids and woven PP geotextile (G1, G2 and G3) for Soil R1 only slightly decreased and it increased in all other cases as a result of the tension associated with the horizontal displacements due to creep and consolidation of the foundation soils.

Figs. 11 and 12 show the mobilized reinforcement stiffness in comparison to the isochronous stiffness from

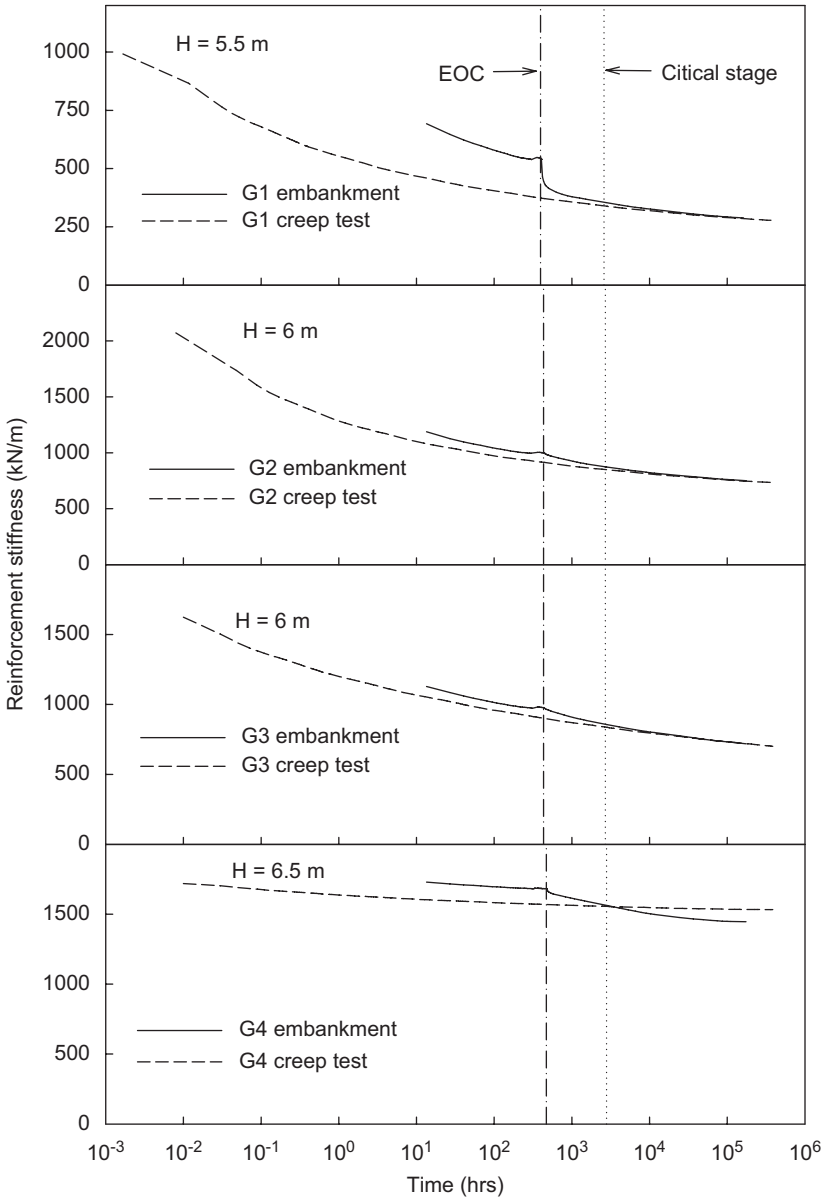

Fig. 12. The variation of reinforcement stiffness with time for embankments over Soil R2.

creep tests. The variation of reinforcement stiffness with time due to creep of reinforcement at constant load was determined through numerical simulations of the creep tests at a constant load corresponding to a mobilized reinforcement force at the critical stage. Thus, they are comparable to the mobilized stiffness after embankment construction as shown in Figs. 11 and 12. For all cases, the mobilized reinforcement stiffness at the end of construction was somewhat higher than the isochronous stiffness. But, it was significantly lower than the initial tensile stiffness for the geogrids and woven PP geotextile (G1, G2 and G3) reinforcement. At the critical stage, the mobilized reinforcement stiffness was practically the same as the isochronous stiffness. This implies that the governing stiffness of reinforcement can be represented by the isochronous stiffness at the critical stage rather than the tensile stiffness measured in tensile tests at a standard rate of 10% min^{-1}.

3.1.2. Foundation deformations due to creep of both reinforcement and foundation soils

Due to the viscous behavior of both the reinforcement and foundation soils, time-dependent deformations of the foundation soil were significant as shown in Figs. 13 and 14. To investigate the time-dependent deformations after construction, Figs. 13 and 14 show the net increase, between EOC and 98% consolidation, in the horizontal deformation of foundation soils below the embankment toe for embankments over the less viscous Soil R1 and more viscous Soil R2, respectively. The horizontal deformations at the end of construction were relatively small for

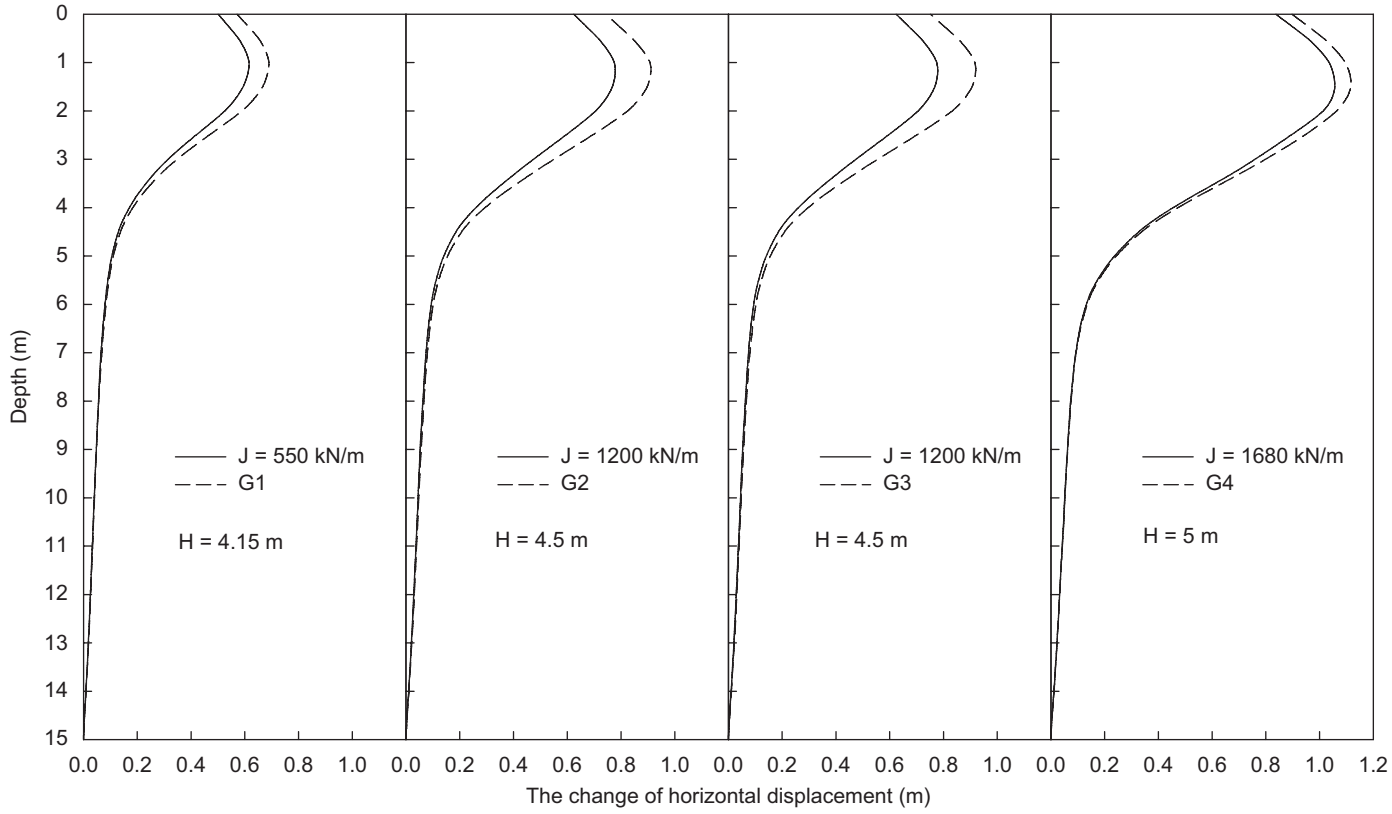

Fig. 13. The change of horizontal deformations below embankment toe between EOC and 98% consolidation for embankments over Soil R1.

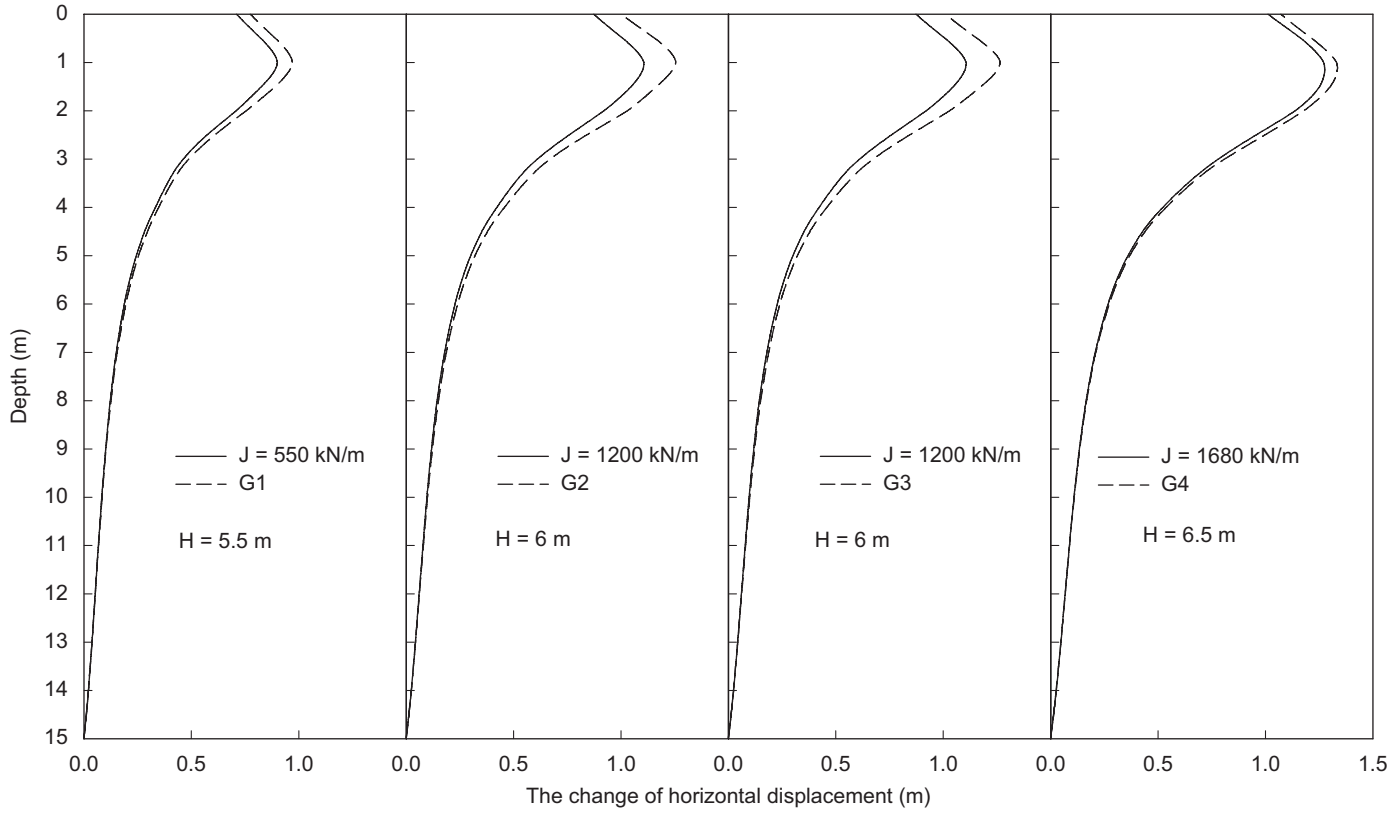

Fig. 14. The change of horizontal deformations below embankment toe between EOC and 98% consolidation for embankments over Soil R2.

Table 4
Calculated embankment heights based on limit states design method

Reinforcement (kN/m)	Embankment height (m)	
	Soil R1	Soil R2
G1		
$J_i = 400$	2.85	3.55
$J_t = 850$	3.05	3.8
G2		
$J_i = 960$	3.1	3.8
$J_t = 1940$	3.45	4.25
G3		
$J_i = 940$	3.1	3.8
$J_t = 1578$	3.33	4.1
G4		
$J_t = 1736$	3.4	4.2

all cases. The difference of horizontal displacement between the case with viscous reinforcement and the case with inviscous reinforcement was relatively small. It is evident that creep and consolidation of the foundation soils dominated the time-dependent deformations and the effect of reinforcement creep was far less significant than that of foundation soils.

3.2. The behavior of reinforcement under working stress conditions

The behavior of reinforcement under working stress conditions is examined using a limit state design approach (Becker, 1996; McGown et al., 1998). The limit equilibrium program REAP (Mylleville and Rowe, 1988) was used to design embankments for a limit equilibrium ratio of 1.0 using factored soil and reinforcement parameters (i.e. the factored resistance equal to factored load). An allowable strain, ε_{all}, of 5% was adopted for the reinforcement. To consider the short-term viscous effect of reinforcement, the isochronous stiffness, J_i, at the critical stage (as shown in Figs. 11 and 12) was used except for the creep insensitive woven PET reinforcement (G4). Since the stiffness from the wide-width tensile tests at a rate of 10% (denoted as J_t) is widely used (GFR Specifier's Guide, 2006), designs based on J_t were also examined. The ratio of J_t to J_i is about 2.1 for the two geogrids (G1 and G2) and 1.7 for the woven PP geotextile (G3). Other partial factors used were $f_{c1} = 1.3$ for the undrained shear strength of the foundation soil, $f_{c2} = 1.0$ for the fill/foundation interface strength, $f_\phi = 1.2$ for both the embankment fill strength and reinforcement/fill interface strength parameters ($\tan\phi$ and $f_\phi = 1.0$ for the unit weight of the embankment fill. The undrained shear strength profiles (prior to application of a partial factor f_{c1}) were theoretically calculated for soils under undrained compression at strain rates of 5×10^{-5} and $1 \times 10^{-5}\,h^{-1}$ (i.e. the critical strain rate) for Soils R1 and R2, respectively, using the soil properties shown in Table 3.

The calculated embankment design heights using REAP (Mylleville and Rowe, 1988) are listed in Table 4. Figs. 15 and 16 show the variation in the maximum reinforcement strain with time up to the time corresponding to 98% degree of consolidation for embankments constructed to their design heights at a rate of 10 m/month. At the end of construction, the reinforcement strains were less than or equal to 0.5% for all cases. The long-term increase of reinforcement strain due to creep of reinforcement and foundation soils was between 0.5% and 1.5% depending on the case. For example, in the case of the 3.1-m high-strength geogrid (G2) reinforced embankment over more viscous Soil R2, the maximum reinforcement strain was 0.4% at the end of construction and the long-term increase of reinforcement strain was about 0.6%. This magnitude of working reinforcement strain has also been observed in field cases. For example, Litwinowicz et al. (1994) report the performance of a 3-m-high PP-reinforced embankment under working conditions, where the long-term increase of reinforcement strain was 0.5% (from 0.5% at EOC).

In general, the increase in reinforcement strain after construction was higher for embankments over the more viscous (rate sensitive) Soil R2 than for embankments over rate the less viscous Soil R1 due to the higher creep deformations developed in the foundation Soil R2. Nevertheless, the total long-term reinforcement strain was less than 2.5% for all cases examined in Figs. 15 and 16. It was found that the effect of reinforcement creep was insignificant during consolidation for embankments over Soils R1 and R2 under working conditions. This was in large part because there was no contiguous plastic failure zone developed in the foundation soil below the embankment for any of the cases examined under working conditions. Since the embankments were stable at the end of construction without the additional resistance from reinforcement, there was practically no creep strains developed in reinforcement during consolidation under working state conditions. This finding differs substantially from that where the full mobilized strength of the foundation soil and a limit strain of 5% were used to calculate the height.

For the design based on $\varepsilon_{all} = 5\%$ and J_i, the long-term reinforcement strain was less than 1.6% (Figs. 15 and 16). This indicates that a design based on factored parameters considering both short- and long-term creeps of reinforcement (i.e. using $\varepsilon_{all} = 5\%$ and J_i) is quite conservative when the in situ undrained shear strength of foundation soils is 1.3 times higher than the factored design strength.

The use of $\varepsilon_{all} = 5\%$ and tensile stiffness J_t resulted in a higher design height and consequent reinforcement strain than the design based on $\varepsilon_{all} = 5\%$ and tensile stiffness J_i. Nevertheless, even in this case, the long-term maximum reinforcement strain was still significantly below the allowable strain.

One additional analysis was conducted to investigate the design based on the factored soil strength and the unfactored reinforcement ultimate strength (i.e. $T_{ult} = 166$ kN/m for the high strength geogrid reinforcement G2). The

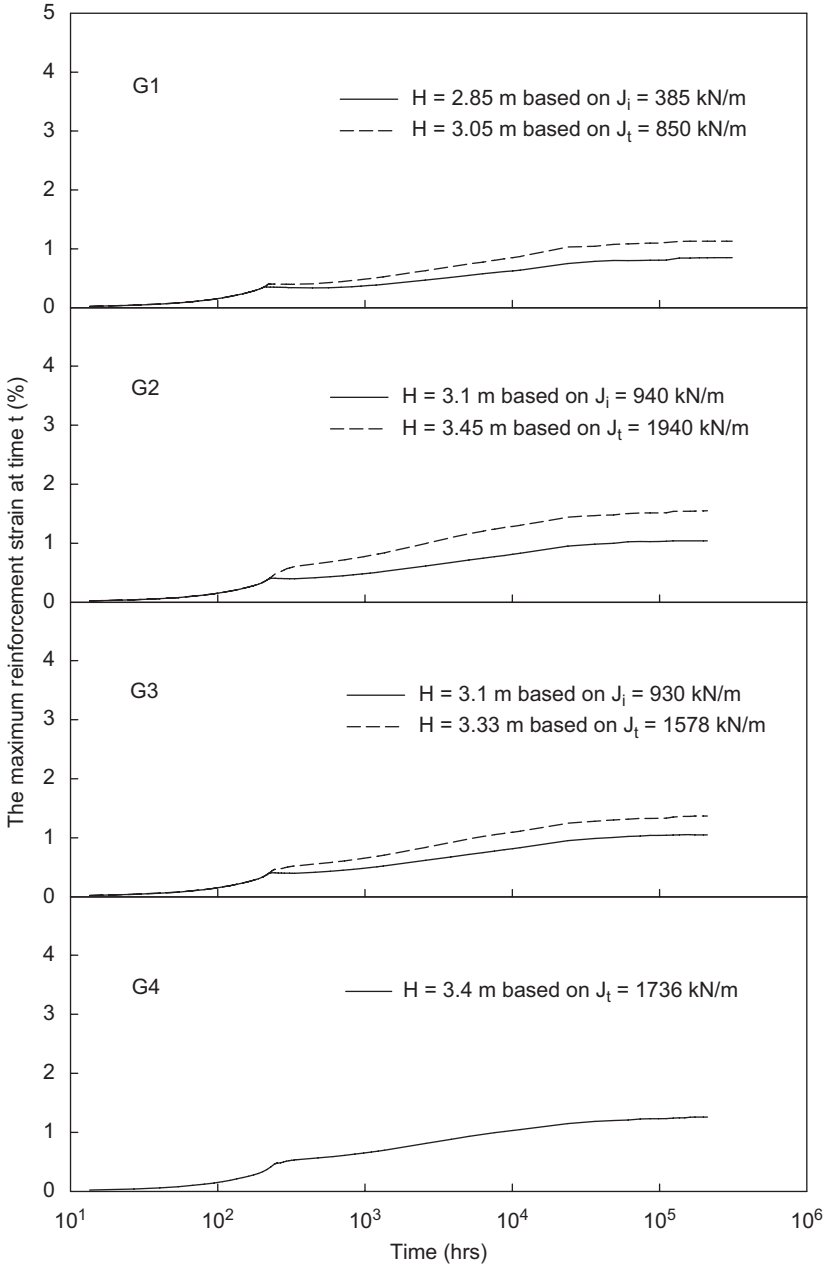

Fig. 15. The variation of reinforcement strain with time for embankments over Soil R1 under working conditions.

corresponding design height was 4.8 m for Soil R2. The total reinforcement strain (shown in Fig. 16) increased significantly after the end of construction although the maximum long-term strain was still only 3%.

For the embankments designed based on undrained limit equilibrium analyses, the long-term reinforcement strains developed were below the allowable strain 5% for all cases examined. This can be attributed to three factors: (1) the strength of foundation soil was higher than the factored strength used in design, (2) the strength gain due to the partial consolidation during construction increased stability and (3) the creep deformations of reinforcement and foundation soils were relatively small at working stress conditions since tension in reinforcement and the shear stresses in the foundation soil were both relatively low. A number of case histories have also shown that the mobilized reinforcement strain or force was lower than the design values (Fowler and Edris, 1987; Duarte and Satterlee, 1989; Bassett and Yeo, 1988; Fritzinger, 1990; Litwinowicz et al., 1994; Loke et al., 1994; Matichard et al., 1994; Varuso et al., 1999).

4. Conclusions

The behavior of geosynthetic-reinforced embankments constructed over rate-sensitive soft foundation soils was investigated for both short- and long-term conditions. The time-dependent behavior of four typical geosynthetic

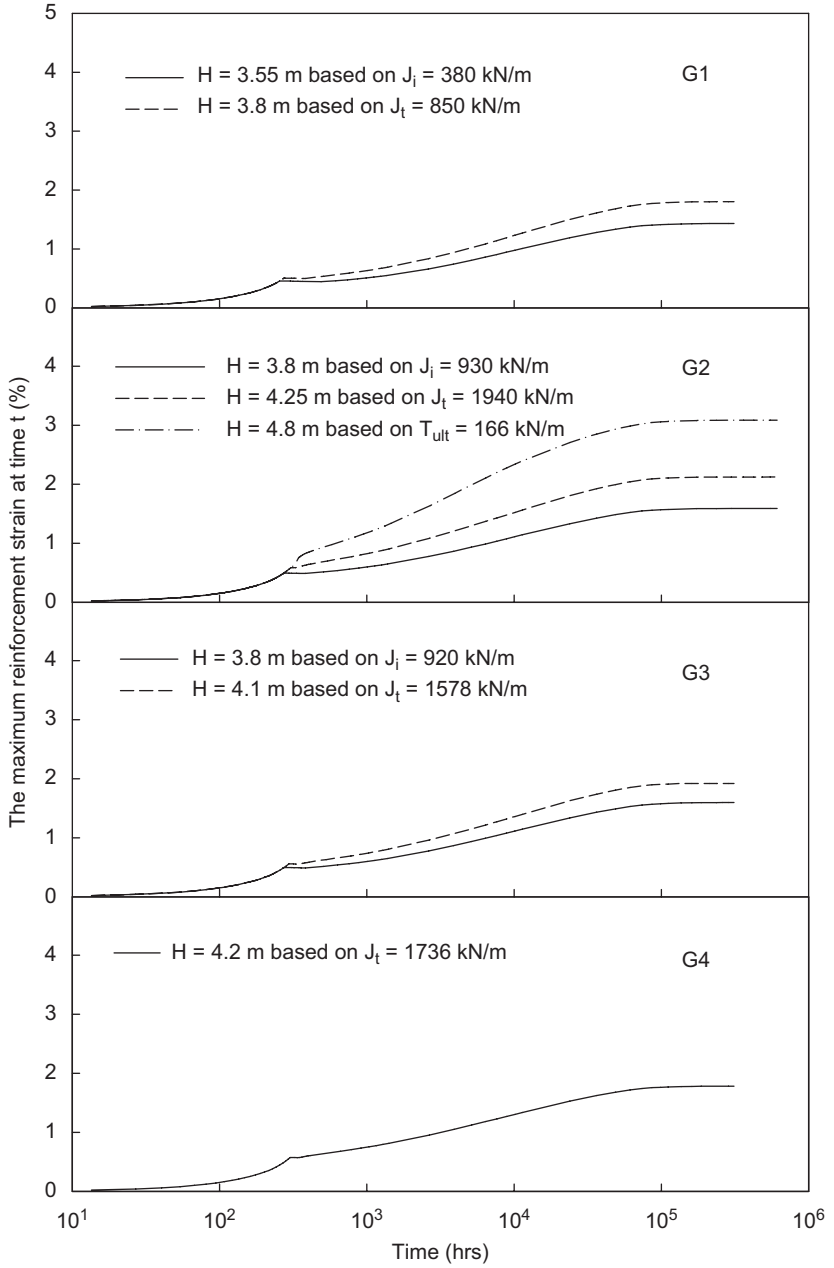

Fig. 16. The variation of reinforcement strain with time for embankments over Soil R2 under working conditions.

reinforcements (i.e. two high density PE geogrids, one woven PP geotextile and one woven PET geotextile) was examined. The creep strain after embankment construction and creep-induced foundation deformations were evaluated for typical rate-sensitive foundation soils. The influence of viscous properties of both the reinforcement and foundation soils were considered. The following conclusions are based on the cases examined and additional research is required before generalizing these beyond this context.

(1) At the critical stage with respect to stability, the mobilized reinforcement stiffness was less than that measured in a laboratory from wide-width tensile tests at a standard rate of $10\%\,\mathrm{min}^{-1}$ for geosynthetic reinforcement exhibiting viscous behavior.
(2) The mobilized reinforcement stiffness at the critical stage is affected by viscoplastic behavior of the foundation soils and the isochronous stiffness measured from the creep tests can reasonably represent the mobilized reinforcement stiffness at the critical stage.
(3) The short-term reinforcement strain increases significantly with time before the critical stage is reached. The long-term reinforcement strain is a function of viscoelastic properties of the reinforcement, the properties of foundation soils and embankment height. However, creep of the foundation soils dominated the

post-construction reinforcement strain for the rate-sensitive foundation soils examined.

(4) The reinforcement force increases with time following the end of construction due to its role in reducing lateral movements of the foundation soil arising from creep of the foundation soils at the critical stage. Stress relaxation in the reinforcement may occur after the critical stage when the stability of the embankment is less dependent on the reinforcing force due to consolidation of the foundation soil.

(5) Embankments whose working height was based on a factored shear strength mobilized at the critical stage (with a partial factor $f_{c1} = 1.3$) and maximum strain of 5% were shown to experience very little creep of reinforcement or foundation soil since the soil was predominantly in an elastic state and there was no contiguous plasticity.

Acknowledgment

The work reported in this paper was funded by the Natural Sciences and Engineering Research Council of Canada.

References

Allen, T.M., 1991. Determination of long-term tensile strength of geosynthetics: a state-of-the-art review. Geosynthetics 91, 351–379.

Allen, T., Vinson, T.S., Bell, J.R., 1982. Tensile strength and creep behavior of geotextiles in cold region applications. In: Proceedings of the Second International Conference on Geotextiles, Las Vegas, USA, vol. III, pp. 775–780.

Bassett, R.H., Yeo, K.C., 1988. The behaviour of a reinforced trial embankment on soft shallow foundations. In: Proceedings of the International Geotechnical Symposium on Theory and Practice of Earth Reinforcement, Fukuoka, Japan, pp. 371–376.

Becker, D.E., 1996. Eighteenth Canadian geotechnical colloquium: limit states design for foundations. Part I. An overview of the foundation design process. Canadian Geotechnical Journal 33 (6), 956–983.

Bergado, D.T., Teerawattanasuk, C., 2008. 2D and 3D numerical simulations of reinforced embankments on soft ground. Geotextiles and Geomembranes 26 (1), 39–55.

Biot, M.A., 1941. General theory of three-dimensional consolidation. Journal of Applied Physics 12, 155–164.

Bjerrum, L., 1972. Embankments on soft ground. In: Proceedings of ASCE Specialty Conference on Earth and Earth-supported Structures, Purdue University, West Lafayette, vol. II, pp. 1–54.

Bonaparte, R., Berg, R., 1987. Long-term allowable tension for geosynthetic reinforcement. In: Proceedings of the Geosynthetic '87 Conference, New Orleans, USA, pp. 181–192.

Bueno, B.S., Costanzi, M.A., Zornberg, J.G., 2005. Conventional and accelerated creep tests on nonwoven needle-punched geotextiles. Geosynthetics International 12 (6), 276–287.

Carter, J.P., Balaam, N.P., 1990. AFENA—A General Finite Element Algorithm: Users Manual. School of Civil and Mining Engineering, University of Sydney, NSW, Australia.

Casagrande, A., Wilson, S.D., 1951. Effect of rate of loading on the strength of clays and shales at constant water content. Géotechnique 2, 251–263.

Chen, W.F., Mizuno, E., 1990. Nonlinear Analysis in Soil Mechanics—Theory and Implementation. Elsevier, New York.

Christopher, B.R., Holtz, R.D., Bell, W.D., 1986. New tests for determining the in-soil stress–strain properties of geotextiles. In: Proceedings of the Third International Conference on Geotextiles, Vienna, Austria, vol. 3, pp. 683–688.

Davis, E.H., 1968. Soil mechanics—selected topics. In: Lee, I.K. (Ed.), Theories of Plasticity and Failure of Soil Masses. Butterworths, p. 1968 (Chapter 6).

Duarte, F.M., Satterlee, G.S., 1989. Case study of a geotextile reinforced levee on a soft clay foundation. In: Proceedings of Geosynthetics '89, San Diego, pp. 160–171.

Fowler, J., Edris Jr., E.V., 1987. Fabric reinforced embankment test section, Plaquemine Parish, Louisiana, USA. Geotextiles and Geomembranes 6, 1–51.

Fritzinger, S.A., 1990. Subaqueous use of high-strength geotextiles. In: Proceedings of the Fourth International Conference on Geotextiles and Goemembranes and Related Products, the Hague, Netherlands, vol. 1, pp. 143–148.

GFR Specifier's Guide, 2006. Geotechnical Fabrics Report, December 2005–January 2006, 23 (9). Industrial Fabrics Association International, Roseville, USA.

Graham, J., Crooks, J.H.A., Bell, A.L., 1983. Time effects on the stress–strain behaviour of natural soft clays. Géotechnique 33, 340–727.

Greenwood, J.H., 1990. The creep of geotextiles. In: Proceedings of the Fourth International Conference on Geotextiles and Goemembranes and Related Products, the Hague, Netherlands, vol. 2, pp. 645–650.

Greenwood, J.H., Myles, B., 1986. Creep and stress relaxation of geotextiles. In: Proceedings of the Third International Conference on Geotextiles, Vienna, Austria, vol. 3, pp. 821–824.

Hinchberger, S.D., 1996. The behaviour of reinforced and unreinforced embankments on rate sensitive clayey foundations. Ph.D. Thesis. Faculty of Graduate Studies, University of Western Ontario.

Hinchberger, S.D., Rowe, R.K., 1998. Modelling the rate sensitive characteristics of the Gloucester foundation soil. Canadian Geotechnical Journal 35 (5), 769–789.

Hinchberger, S.D., Rowe, R.K., 2003. Geosynthetic reinforced embankments on soft clay foundations: predicting reinforcement strain at failure. Geotextiles and Geomembranes 21 (3), 151–175.

Janbu, N., 1963. Soilompressibility as determined by oedometer and triaxial tests. In: Proceedings of the European Conference on Soil Mechanics and Foundation Engineering, Wiesbaden, Germany, vol. 1, pp. 19–25.

Jewell, R.A., Greenwood, J.H., 1988. Long term strength and safety in steep soil slopes reinforced by polymer materials. Geotextiles and Geomembranes 7, 81–118.

Kulhawy, F.H., Mayne, P.W., 1990. Manual on estimation soil properties for foundation design. EPRI Report.

Leroueil, S., Marques, M.E.S., 1996. Importance of strain rate and temperature effects in geotechnical engineering. In: Proceedings of the 1996 ASCE National Convention, Washington DC, USA, Geotechnical Special Publication no. 61, pp. 1–60.

Leshchinsky, D., Dechasakulsom, M., Kaliakin, V.N., Ling, H.I., 1997. Creep and stress relaxation of geogrids. Geosynthetics International 4 (5), 463–479.

Li, A.L., Rowe, R.K., 2001. Influence of creep and stress-relaxation of geosynthetic reinforcement no embankment behaviour. Geosynthetics International 8 (3), 233–270.

Li, A.L., Rowe, R.K., 2002. Some design consolidations for embankments on rate sensitive soils. ASCE Journal of Geotechnical and Geoenvironmental Engineering 128 (11), 885–897.

Litwinowicz, A., Wijeyakulasuriya, C.V., Brandon, A.N., 1994. Performance of a reinforced embankment on a sensitive soft clay foundation. In: Proceedings of the Fifth International Conference on Geotextiles, Geomembranes and Related Products, Singapore, September, vol. 1, pp. 11–16.

Loke, K.H., Ganeshan, V., Werner, G., Bergado, T.D., 1994. Fifth International Conference on Geotextiles, Geomembranes and Related Products, Singapore, vol. 1, pp. 25–28.

Matichard, Y., Tanays, E, Carbon, M., 1994. Geotextile reinforced embankment to cross a peat-bog. In: Proceedings of the Fifth

International Conference on Geotextiles, Geomembranes and Related Products, Singapore, vol. 1, pp. 37–40.

McGown, A. Andrawes, K.Z., Kabir, M.H., 1982. Load-extension testing geotextiles confined in-soil. In: Proceedings of the Second International Conference on Geotextiles, Las Vegas, USA, vol. III, pp. 793–798.

McGown, A., Andrewes, K.Z., Pradhan, S., Khan, A.J., 1998. Limit state design of geosynthetic reinforced soil structures. In: Proceedings of the Sixth International Conference on Geosynthetics, pp.144–179.

Mylleville, B.L.J., Rowe, R.K., 1988. Simplified Undrained Stability Analysis for Use in the Design of Steel Reinforced Embankments on Soft Foundations. Faculty of Engineering Science, University of Western Ontario, GEOT-3-88, 73p.

Perzyna, P., 1963. The constitutive equations for work-hardening and rate sensitive plastic materials. In: Proceedings of Vibrational Problems, Warsaw, vol. 4 (3), pp. 281–290.

Rowe, R.K., Hinchberger, S.D., 1998. The significance of rate effects in modelling the Sackville test embankment. Canadian Geotechnical Journal 35 (3), 500–516.

Rowe, R.K., Li, A.L., 2002. Behaviour of reinforced embankments on soft rate-sensitive soils. Géotechnique 52 (1), 29–40.

Rowe, R.K., Soderman, K.L., 1987. Stabilization of very soft soils using high strength geosynthetics: the role of finite element analyses. Geotextiles and Geomembranes 6 (1–3), 53–80.

Rowe, R.K., Taechakumthorn, C., 2008.Combined effect of PVDs and reinforcement on embankments over rate-sensitive soils. Geotextiles and Geomembranes, 26, in press, doi:10.1016/j.geotexmem.2007.10.001.

Sarsby, R.W., 2007. Use of 'Limited Life Geotextiles' (LLGs) for basal reinforcement of embankments built on soft clay. Geotextiles and Geomembranes 25 (4/5), 302–310.

Sheahan, T.C., Ladd, C.C., Germaine, J.T., 1996. Rate-dependent undrained shear behaviour of saturated clay. Journal of Geotechnical Engineering 122 (2), 99–108.

Shrestha, S.C., Bell. J.R., 1982. Creep behavior of geotextiles under sustained loads. In: Proceedings of the Second International Conference on Geotextiles, Las Vegas, USA, vol. III, pp. 769–774.

Soga, K., Mitchell, J.K., 1996. Rate-dependent deformation of structured natural clays. In: Proceedings of the 1996 ASCE National Convention, Washington DC, USA, Geotechnical Special Publication No. 61, pp. 243–257.

Varuso, R.J., Grieshaber, J.B., Nataraj, M.S., 1999. Design and analysis of a geosynthetic levee test section. In: Proceedings of Geosynthetics '99, Boston, USA, pp. 451–464.

Varuso, R.J., Grieshaber, J.B., Nataraj, M.S., 2005. Geosynthetic reinforced levee test section on soft normally consolidated clays. Geotextiles and Geomembranes 23 (4), 362–384.

Zhang, C., Moore, I.D., 1997. Nonlinear mechanical response of high density polyethylene. Part II: uniaxial constitutive modelling. Polymer Engineering and Science 37 (2), 414–420.

Zienkiewicz, O.C., 1977. The Finite Element Method, third ed. McGraw-Hill, New York.